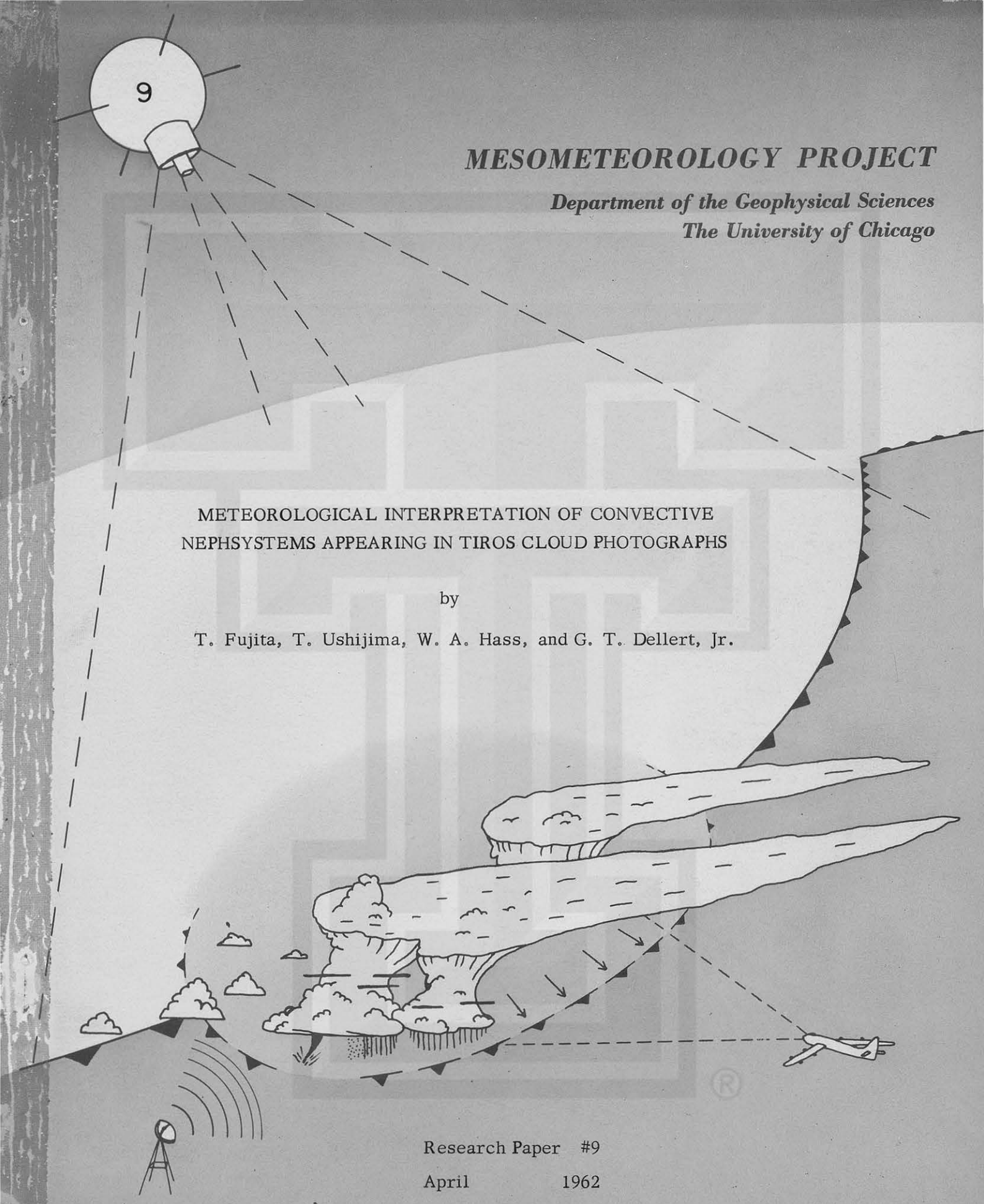

MESOMETEOROLOGY PROJECT

Department of the Geophysical Sciences
The University of Chicago

METEOROLOGICAL INTERPRETATION OF CONVECTIVE NEPHSYSTEMS APPEARING IN TIROS CLOUD PHOTOGRAPHS

by

T. Fujita, T. Ushijima, W. A. Hass, and G. T. Dellert, Jr.

Research Paper #9

April 1962

RESEARCH PAPER #9

MESOMETEOROLOGY PROJECT
Department of the Geophysical Sciences
The University of Chicago

METEOROLOGICAL INTERPRETATION OF CONVECTIVE NEPHSYSTEMS APPEARING IN TIROS CLOUD PHOTOGRAPHS

by

Tetsuya Fujita and Toshimitsu Ushijima - University of Chicago*
William A. Hass and George T. Dellert, Jr. - U. S. Weather Bureau**

Presented before the International Symposium
on Rocket and Satellite Meteorology
April 23-25, 1962
Washington, D.C.

*The research performed at the University of Chicago has been sponsored by the Meteorological Satellite Laboratory, United States Weather Bureau under contract Cwb 10215.

**Mesometeorology Research Project, Meteorological Research Projects Branch, United States Weather Bureau.

TABLE OF CONTENTS

A b s t r a c t

In an effort to utilize Satellite data in research on mesometeorological phenomena, cloud photographs from selected Tiros I and III orbits were rectified precisely. The nephsystems were then studied in combination with other meteorological data such as radar echoes, mesoanalysis charts produced by machine through objective methods, and the radiation data in Channel 2 and 5 from Tiros III. It became evident that Tiros data is precise enough to be used in the quantitative analysis of mesoscale meteorological systems which, on many occasions are omitted or undetected in our regular synoptic analyses.

I. INTRODUCTION

Since the successful launch of Tiros I weather satellite, cloud photographs from an altitude over 400 miles above the surface of the earth have become extremely useful in both operational and research analysis of nephsystems in regular synoptic scales. A pioneering research analysis of Tiros I photographs was made by Fritz and Wexler (1960) leading them to point out the existence of a spiral band structure of extra-tropical cyclones. Also found were various features of nephsystems which had been unknown to us, due to the fact that observations in the past usually were made while looking up.

One of the earliest works relating Tiros cloud photographs to meteorological disturbances in the mesoscale appears in an article by Whitney and Fritz (1961), who investigated the square-looking cloud over the Texas-Oklahoma border.

Attempts to investigate Tiros cloud patterns in combination with associated radar echoes were made by Blackmer (1961), and Fujita and Ushijima (1961), who found that the areas of radar echoes are much smaller than those of clouds. The ratio of the areas

of clouds to echoes was computed in order to learn their variation as a function of time past the first echo appearance.

As far as the investigation of surface pressure patterns in relation to Tiros cloud photographs is concerned, there has not been a good case study that has clarified the relationship between the cloud and pressure patterns. In his recent study on numerical mesoanalysis, Dellert (1962) developed a method of obtaining the mesoscale pressure patterns objectively by using an electronic computer. The objective analysis scheme used in producing pressure maps appears later (section 3), and it will be seen that the patterns produced by a machine are of suitable quality to be related with Tiros cloud patterns.

After the launch of Tiros II, radiation data from the satellite-borne scanning radiometer became available to us. The data provides new ways of depicting the energy emitted or reflected from the subsatellite objects in various scales.

Stroud (1961) quantitatively analysed the patterns of radiation in five channels of Tiros II, orbit 88. They are (1) Water Vapor Channel (6.0-6.5 microns); (2) Atmospheric Window Channel (8-12 microns); (3) Albedo Channel (0.2-6.0 microns); (4) Thermal Channel (8-30 microns); (5) Narrow-Band Visible Channel (0.55-0.75 micron). This orbit, unfortunately, provided no usable cloud photographs. In Channel 2 radiation patterns, a cold region of approximately 200 x 200 miles over the Atlas Mountains, North Africa was found, leading him to imagine that it was an area of clouds. He then pointed out the feasibility of estimating the heights of clouds from the Channel 2 data. On the other hand, Channel 5 patterns indicated a poor resemblance to the other channels leading him to suspect that reflected solar energy varies considerably with the elevation angle of the sun. Large synoptic-scale patterns of Channel 2, Tiros II data was analysed by Fritz and Winston (1962) who successfully estimated the heights of nephsystems in synoptic scales.

Nordberg, Bandeen, Conrath, Kunde and Persano (1962) made a preliminary investigation of Tiros III data with the emphasis on the regular synoptic scale radiation and cloud patterns. Three cases, one over the Northeast coast of South America; another over Eastern United States; and the third over Central Sudan, were investigated in order to learn the usefulness of radiation data for various purposes. They found

that the Channels 3 and 5 data are capable of distinguishing certain terrain features when the region is cloud-free. The Channel 2 data which has been assumed to be relatively free from absorption was found to be affected by water vapor in the atmosphere by as much as 25 percent except over desert areas.

These researches on Tiros data in synoptic scales presented the feasibility of investigating mesoscale meteorological systems with the use of radiation data. Since a large-synoptic scale chart tells us little about the mesoscale systems which are to be related to the radiation patterns, it has become necessary to identify the sources of radiation or reflection directly on the Tiros cloud photographs.

II. TIROS CLOUD PHOTOGRAPHS AND ASSOCIATED RADAR ECHOES

The cloud photographs from Tiros I, orbit 817 passing from Midwestern United States to Florida show the features of both isolated and groups of cumulonimbi. Several frames from tape-mode photographs were rectified to be studied, in detail, together with other meteorological data.

A. Synoptic Situation of May 27, 1960

Midwestern United States on May 27, 1960 when Tiros I, orbit 817 passed over the area was under the influence of a high pressure ridge following a continental cyclone moving eastward over the Great Lakes area. A crude sketch of the cloud patterns obtained from this orbit between 2318 and 2325 GMT appears in Fig. 1. There were a number of isolated cumulonimbi over Florida and nearby waters and almost all of them were accompanied by plumes of faint clouds, extending from the cloud core in the direction of the 300-mb winds.

On the contrary, the horizontal dimensions of the convective clouds over the Midwest were so large that they probably consisted of a large number of convective

towers which cannot be separated into individual elements.

The synoptic situation over the area of cloud analysis is presented in Figs. 2 and 3 which include surface isobars, winds, amount of both low and high clouds; 850-mb winds and isotherms; and the 300-mb-height contours. The charts reveal that the area of isolated cumulonimbi was located within the warm sector east of a cold front extending southward from the cyclone center over the Greak Lakes region. The direction of the 300-mb winds and that of the plumes from isolated cumulonimbi was very close, suggesting that they originated from the active portion of each cloud.

Appreciable differential warm advection from the south is apparent near the western edge of the chart, where large masses of nephsystems were observed. One might not imagine the existence of several mesoscale nephsystems in elliptic shapes, just by analysing the distribution of the amount of clouds given in the synoptic charts. There was a zone of clear areas over the high pressure ridge separating the cyclone nephsystem to the northeast and the masses of convective ones.

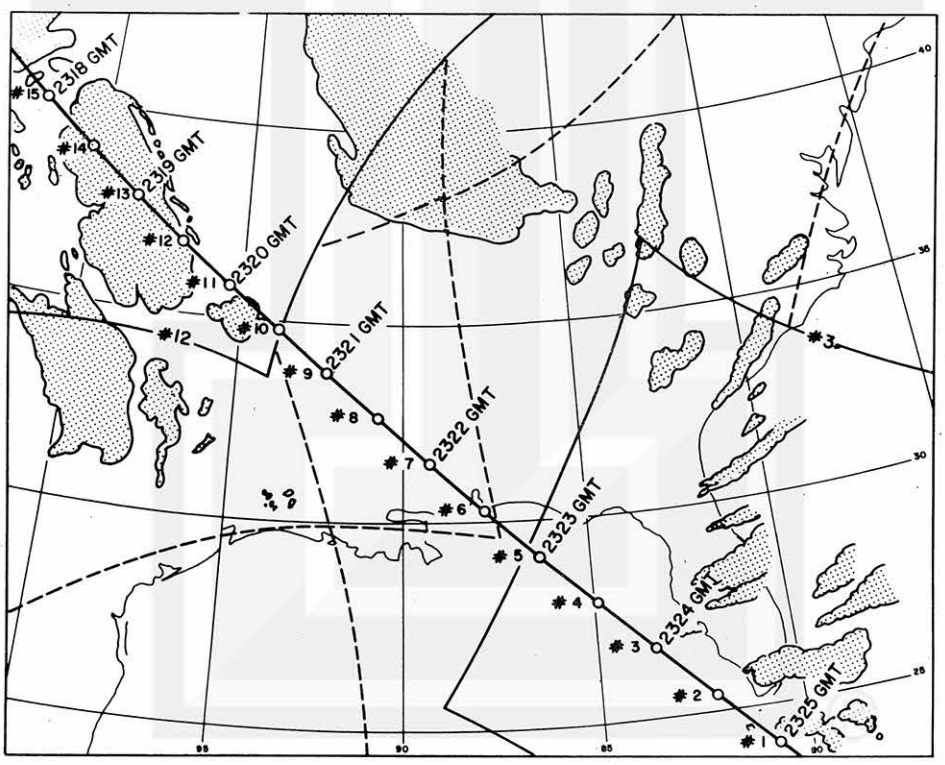

Fig. 1 Terrestrial satellite-subpoint track of Tiros I, orbit 817 on May 27, 1960. Numbers entered along the track are tape-mode frame numbers. Stippled areas represent cloud areas obtained from the four pictures rectified with high accuracy.

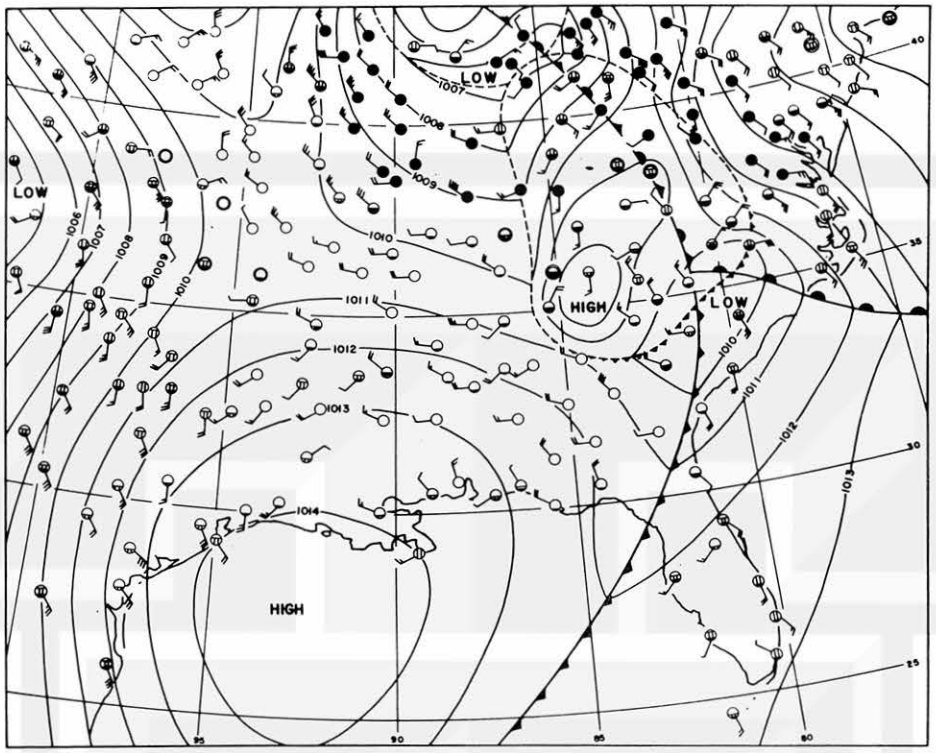

Fig. 2 Surface chart for 2400 GMT, May 27, 1960. The amount of low and other clouds are represented by hatched and painted areas below the horizontal lines in each station circle. The height of the horizontal lines above the bottom of the circle is proportional to the cloud cover. Each long barb in wind symbols denotes 5-kts wind speed.

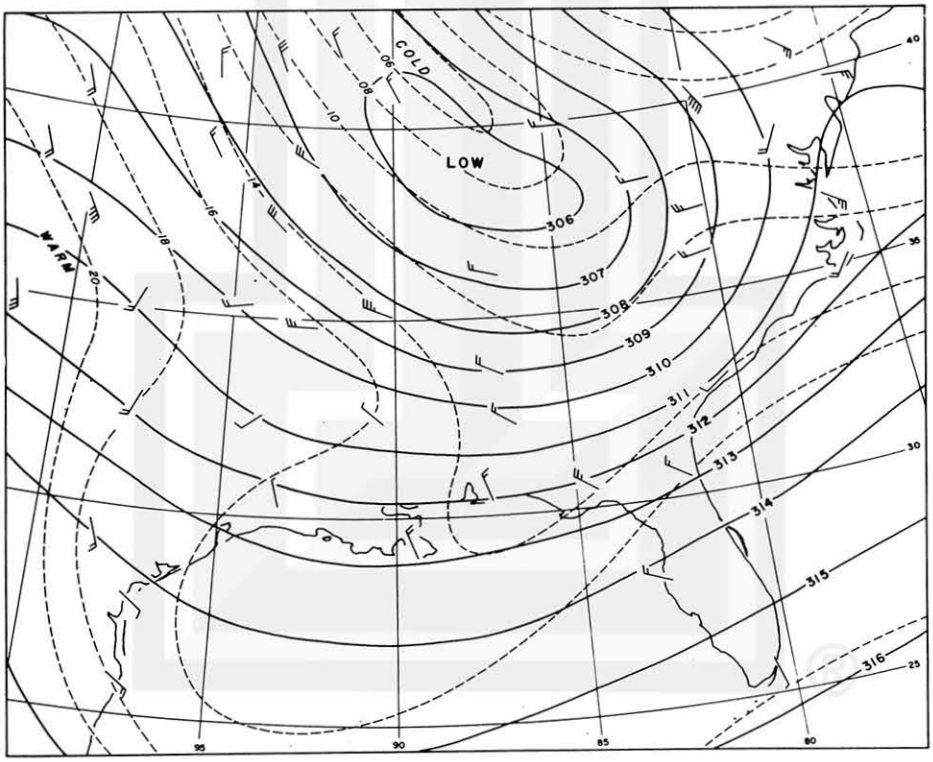

Fig. 3 Upper-air chart for 2400 GMT, May 27, 1960. The 850-mb winds and isotherms drawn at every 2°C intervals are superimposed on the 300-mb winds and height contours.

B. Isolated Cumulonimbi over Florida and Nearby Waters

Tiros cloud photograph frame #3 showing isolated cumulonimbi over Florida was exposed at 2324 GMT (1824 EST). Fortunately, the large portion of the area of cumulonimbus convection was covered by the WSR-57 radar at Miami photographed at 1821 EST, only a few minutes before the time of the Tiros photograph. For their comparison, both Tiros and radar pictures are shown in Figs. 4 and 5. The range markers on the radar photograph are at 50-N.M. intervals. There were about 100-precipitation cells within the 250-nautical miles of Miami radar. Most of these cells were more or less scattered over a large area without showing organized patterns.

The Tiros photograph, however, revealed the existence of about 16 convective nephsystems within the same range as that of the radar photograph. Each nephsystem, therefore, included an average of 6-precipitation cells. The relationship between radar echoes and clouds seen in Tiros photographs are better understood by examining Fig. 6, in which each cumulonimbus system is numbered. System No. 3 located off the west coast of Florida was seen on the radar scope as two isolated echoes, about 3 miles in diameter. Each echo was accompanied by a plume of about 25 miles in length and first appeared on the radar scope approximately one hour before the time of the Tiros photograph. On the other hand, the 3 hour-old systems such as 1 and 2 were characterized by plumes extending over 80 miles.

The plumes under discussion are very similar to those studied by Hitschfeld (1960) using CAPPI-radar data. They are characterized by the typical long anvils developing under a severe vertical wind shear. If we assume that the fall velocity of ice crystals from the anvil tops is relatively low and uniform, the formula used by Hitschfeld,

$$\Delta S = (W - W_c) \frac{\Delta z}{v}$$

where ΔS is the horizontal displacement of a particle falling with a speed, v, through a layer of thickness, Δz, can be reduced to

$$\Delta S = (W - W_c) \Delta t ,$$

Fig. 4 Radar echoes at 1821 EST, May 27, 1960 photographed with WSR-57 radar at Miami. Range markers are at 50 N.M. intervals.

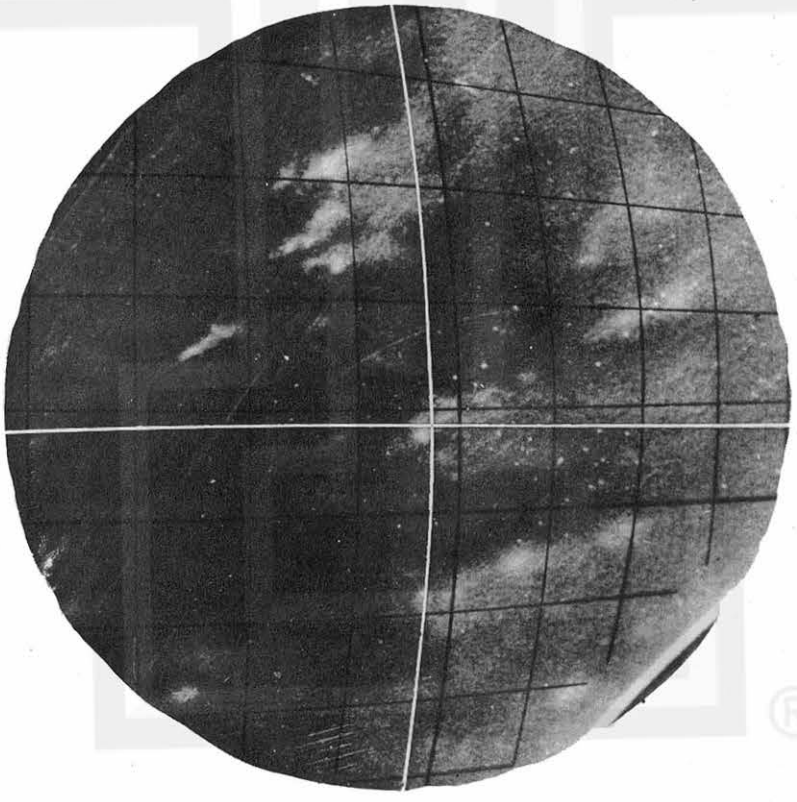

Fig. 5 Tiros cloud photographed at 1824 EST, May 27, 1960. The photograph covers the area within 250 N.M. of Miami, located at the intersection of the white lines.

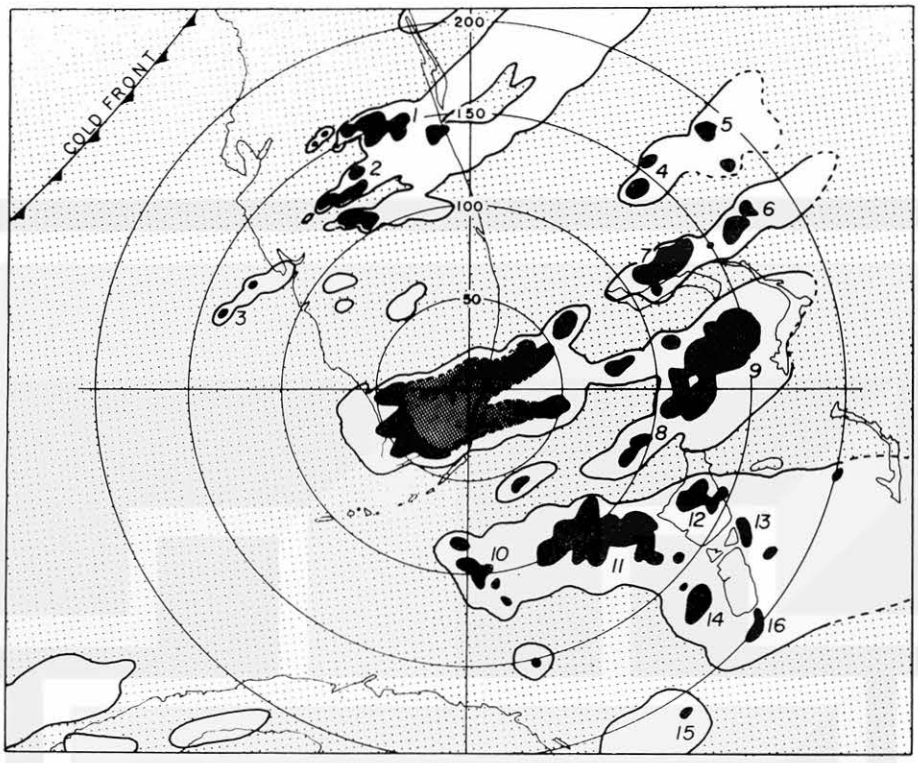

Fig. 6 Composite of Tiros cloud patterns (1824 EST) and WSR-57 radar echoes (1821 EST).

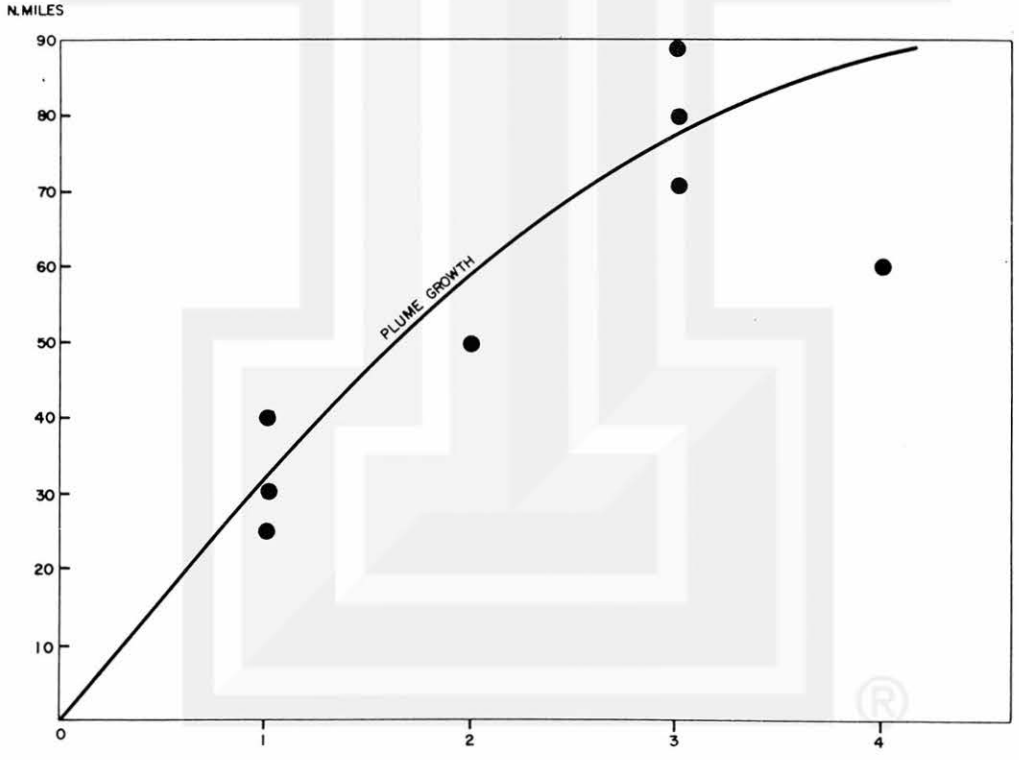

Fig. 7 Growth rate of plumes from cumulonimbi of May 27, 1960 over Florida. The plumes first grew with the velocity of horizontal winds at the cloud-top levels. As the time passed, ice crystals sublimated and diffused, resulting in a slower rate of plume growth.

by substituting v by $\Delta z / \Delta t$. W and Wc in the formula are the velocity of wind at the anvil level and that of the cloud. This indicates that the length of an anvil is proportional to the time past the anvil initiation.

Nephsystem number	1	2	3	4	5	6	7	8	9	10	11	12	13	14
Time past initiation (hr)	3	3	1	2	1	4	1	2	2	?	3	1	1	1
Length of plume (N. M.)	80	90	25	50	30	60	40	?	?	?	70	40	?	?

Table I. The length of cirrus plume and the time past the initiation of radar echo tabulated for each nephsystem number appearing in Fig. 6.

The plume lengths given in Table I were plotted against the period of radar echoes observed prior to the time of the cloud photographs. The result in Fig. 7 indicates that the anvil lengths grew, at the expected rate derived from the above formula, during the first hour or so, then their growth rate decreased considerably.

Incidentally the echoes over Florida moved at the rate of about 40 kts from the WSW while the winds at the 200-mb level were 80 kts (Miami) and 66 kts (Tampa). The motion of the 200-mb winds relative to the clouds, therefore, was about 32 kts.

Such a decrease in rate of anvil growth is probably due to the diffusion and sublimation of ice crystals which reduce the reflectivity of light from the anvil tops resulting in shorter anvils than expected from linear growth.

C. Massive Squall Nephsystems Over the Midwest

The massive squall nephsystems over the Midwest which will be discussed are the ones studies by Blackmer (1961). He stated that the cloud areas in Tiros photographs are much larger than those of radar echoes, because the cloud boundary includes the entire cirrus deck covering the cloud tops.

Of extreme interest is the massive appearance of these squall nephsystems, which

is quite different from the plume shaped anvils over Florida. There were no streaks separating the anvils from individual convective towers, and the cloud appeared to be a huge deck of cirrus or cirrostratus mushrooming over the area of activity.

Now, we shall examine the radar photograph in Fig. 8 together with the satellite cloud photograph of Fig. 9. The former was photographed at 1715 CST, four minutes before the Tiros photograph; these photographs are considered to be simultaneous from our analysis point of view. In view of the sharp drop in echo intensity along the western edge of the echoes and of the existence of minor echoes beyond the range of the major nephsystems, there probably was insignificant attenuation. The radar was CPS-9 with 3-cm wavelength located at Shilling Air Force Base, Kansas.

The cloud photograph, as well as radar photograph, reveals the sharp drop in light reflectivity along the western edge of the nephsystem. We may postulate that such a distinct and sharp edge was accentuated by the dry air descending along the slope of the Rocky Mountains. Such a phenomenon is very common in the extreme western part of the Midwest.

Figure 10 includes both cloud patterns and radar echoes in two-intensity contours. The 850-mb winds beneath the massive nephsystems, which were the major source of the low-level moisture inflow were south-southeast about 15kts; and the area of clouds was under the influence of strong differential warm advection. The vertical distribution of this warm advection is represented by the sounding from Oklahoma City located near the southeastern edge of the clouds under discussion. The wind velocity hodograph in Fig. 11 reveals the existence of intense warm advection between the surface and the 700-mb level where the lapse rate was dry-adiabatic. This layer and mean warm advection is indicated by "A". Above this layer, there existed a layer of weak warm advection shown as "B", which was caused by non-adiabatic heating and the transport of dry air over the Rocky Mountains. On top of this dry heated air, westerlies with moderate vertical wind shear were prevailing with a maximum speed of about 50 kts at the 250-mb level.

The upper-air structure, radar-echo distribution, and the Tiros cloud photograph combined into mesosynoptic analysis permit us to estimate the formation process of the massive nephsystems as follows: a localized break-through of moisture first takes

Fig. 8 Echoes at 1715 CST, May 27, 1960 photographed with CPS-9 radar located at Shilling Air Force Base, Kansas. The range markers are at 50-mile intervals.

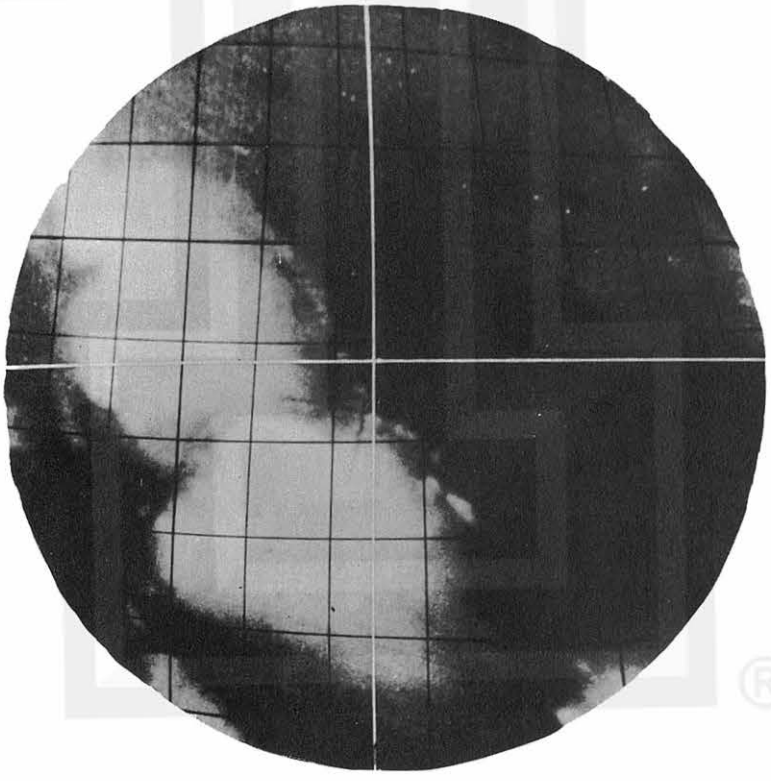

Fig. 9 Tiros cloud photograph exposed at 17h 19m 30s, May 27, 1960. Longitudes and latitudes were drawn on the photograph at one-degree intervals.

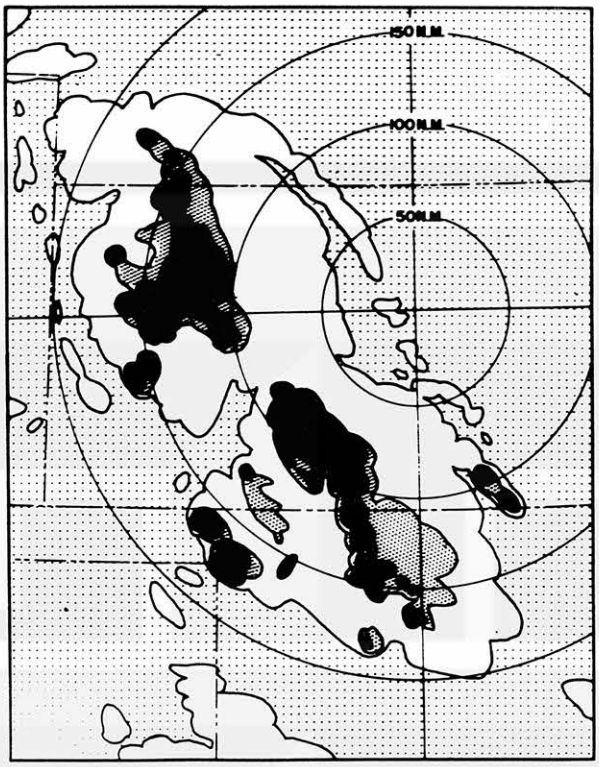

Fig. 10 Composite representation of Tiros cloud photograph (1719 CST) and CPS-9 radar echoes (1715 CST) represented in two-intensity contours.

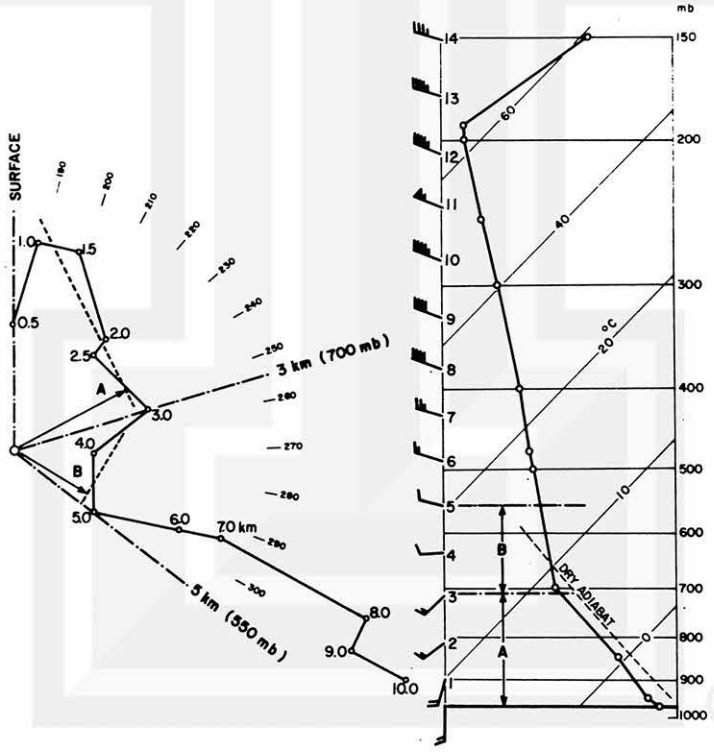

Fig. 11 Upper-air sounding from Oklahoma City at 1800 CST, May 27, 1960. The sounding was made about 40 minutes after the Tiros photograph, while the east edge of the nephsystem was mushrooming over the station. Left figure is the hodograph of winds up to the 10-km level. There was intense warm advection between the surface and the 2-km level.

place over an area of intense warm advection below the 700-mb level. The middle levels of the convective clouds along the western edge undergo continuous but slow erosion by dry warm air from the Rocky Mountains; meanwhile, the ice crystals from the cloud tops spread out toward the downwind side of the 250-mb wind. Areal coverage of Tiros cloud photographs suggests that the cirrus decks may even move westward relative to the convective towers.

III. MACHINE-PRODUCED MESOANALYSIS CHARTS AND TIROS NEPHSYSTEMS

A. Objective Mesoanalysis of Surface Pressure

The machine-produced mesoscale, surface analyses of the central United States area photographed by the Tiros I satellite on May 27, 1960, were obtained in the manner described previously by Dellert (1962). In summary, the procedure was as follows:

Microbarograms for the 12-hour period from 1200 CST, May 27, 1960, to 0000 CST, May 28, 1960, were placed on punch cards, using a Benson-Lehner Oscar "K" trace reader. Microbarograms for all severe storm research network stations in Kansas, Oklahoma, and the Texas Panhandle were used and all first order stations in the area bounded by Latitudes 31.5^{o}N and 42^{o}N, Longitudes 90^{o}W and 106^{o}W, including northern Texas, Oklahoma, Kansas, Nebraska, eastern Colorado, eastern New Mexico, southern Iowa, Missouri, and Arkansas.

As the traces were loaded into the computer the time-station pressure data were adjusted for fast or slow clocks and skewed microbarograms. The traces were then scanned by the machine to determine the greatest disturbance in the traces and the least disturbed three-hour period common to all traces in the 12-hour period of analysis.

The program found that the fastest and greatest pressure rise occurred at Kinsley,

Kansas, at 2018 CST, almost exactly three hours after the Tiros satellite photographs of this area.

The objective analysis scheme used in producing the maps shown here consists of finding the nearest three stations to the particular grid point for which P* value (sea level pressure) is desired. These three stations are selected to form an enclosing triangle about the grid point. A plane is fitted to the P* values at the three stations and the P* value of this plane at the location of the grid point is obtained. In effect, pressure traces are thus synthesized for each point on the grid, although at this stage of development of the program the traces synthesized are subject to undesirable smoothing.

The least disturbed period common to all stations was the first three hours of the period of analysis, from 1200 CST to 1500 CST on May 27. The smoothed and averaged map drawn for this period (Fig. 12), based on the first order stations only, agreed very well with the 1200 CST NMC sea level analysis, indicating an intense ridge extending from northern Louisiana north-northwestward into eastern Kansas, with fairly strong southerly flow over the western portion of Kansas and Oklahoma. There were some indications of a weak trough extending in an east-west direction along the Kansas-Oklahoma border west of the ridge, and another east-west trough through central Nebraska. Both of these corresponded fairly well with the positions of two of the cloud systems observed later by the satellite and, since they show up in a three-hourly averaged analysis, they were felt to be significant.

The research network stations are not surveyed and actual station pressure recorded by them is somewhat uncertain. They are calibrated from the three-hour smoothed map. The three-hour mean P* value for each network station is obtained from the mean P* values of three nearby first order stations by the objective analysis portion of the program in precisely the same manner as each grid point was analyzed to produce the smoothed map. The difference between this computed mean P* value and the three-hour mean station pressure for the network station is then added to all of the recorded pressures for the station's trace to form the sea level (P*) trace used in producing the detailed pressure charts.

The detailed analysis at 1400 CST (Fig. 13) shows the extent of the development of the trough extending along the Kansas-Oklahoma border which was indicated on the

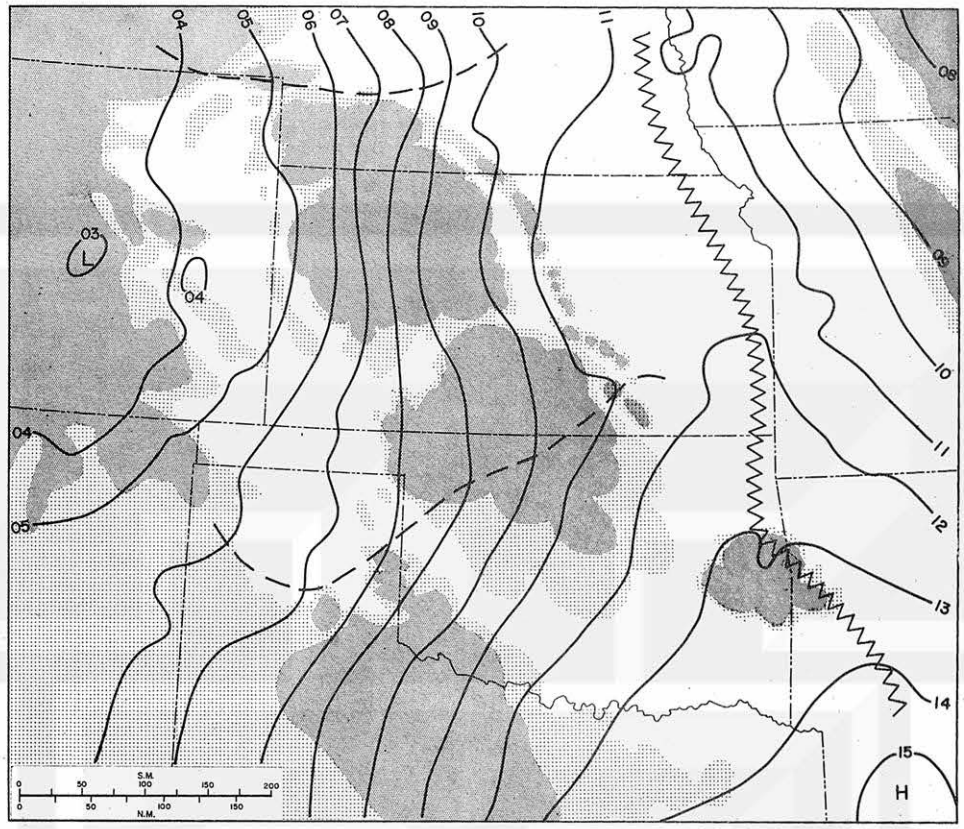

Fig. 12 Smoothed and averaged 3-hourly surface pressure map, 1200 CST to 1500 CST, May 27, 1960. Shaded areas represent cloud photographed at 1719 CST by Tiros I. Isobars are for 1-mb intervals, with labels for units and tens ("12" for 1012 mb).

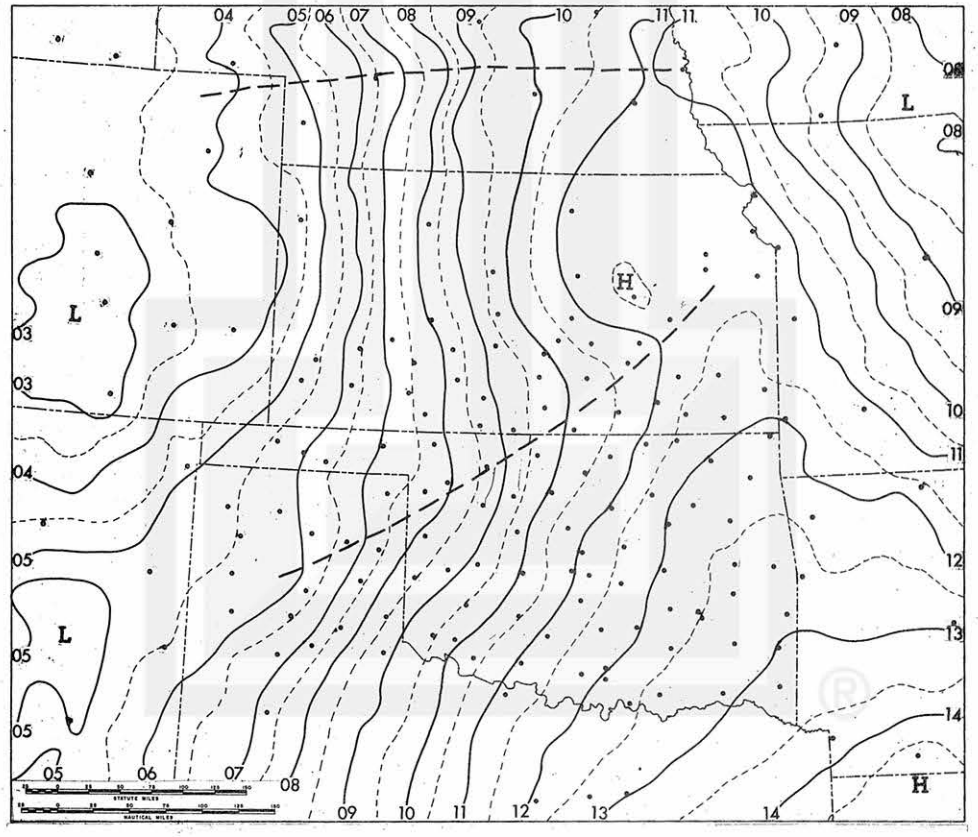

Fig. 13 Machine-produced surface pressure analysis, 1400 CST, May 27, 1960. Locations of regular Weather Bureau and research network stations used in the analyses are shown.

smooth three-hourly map. At 1600 CST (Fig. 14) that trough has broadened but is also broken up by the development of high pressure areas within it, particularly the sharp ridge over south-central Kansas. By the time of the Tiros photograph, 1719 CST, a small closed high pressure cell has formed and appears directly under the southern cloud mass (Fig. 15). Another small closed high and a distinct bulge in the main pressure ridge is also apparent under the cloud mass over the Oklahoma-Arkansas border.

Because of the weakness of these systems as revealed by the machine analysis, it was necessary to resort to pressure change charts to follow their development. Such charts were prepared initially on an hourly basis, between 1500 CST and 1900 CST, and indicated a movement of approximately 27 knots east-northeastward for the developing high pressure area along the Kansas-Oklahoma border. This compared favorably with a movement of about 22 knots in the same direction determined from the radar echoes related to this same cloud mass by Blackmer (1961). The pressure change charts also indicated a maximum development in the period 1700-1800 CST (Fig. 16). A further refinement to 20-minute intervals showed that the majority of that hourly change took place between 1730 and 1750 CST.

Referring again to Fig. 15, a heavy line shows the location of a short pressure jump line just in advance of the small high pressure cell over the Kansas-Oklahoma border at the time of the cloud pictures, as evidenced by the pressure traces. Using the rate of movement of 27 knots determined from the pressure change analysis, which is based on a longer history than is available for the pressure jump, the intensity of the jump at this time indicated a gradient of the order of 1.5 mb in one to four miles along the central portion of the line. Further examination of the traces in this particular area by hand mesoanalysis, showed that a more intense high pressure cell existed just north of the cell shown at 1719 CST, between stations, with a central value of about 2 mb greater than that indicated by the machine analysis. This high pressure is reflected in later machine analyses as the cell passed over stations in its path.

The general lack of intensity of the pressure systems analyzed by the program

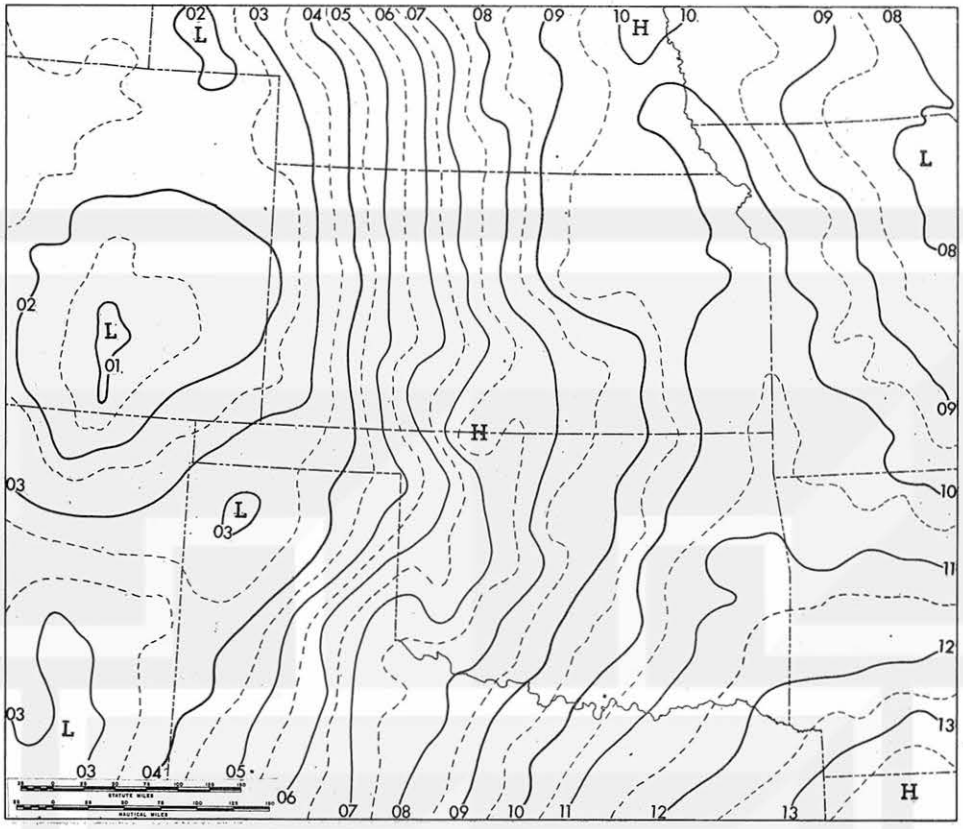

Fig. 14 Machine analysis at 1600 CST, May 27, 1960.

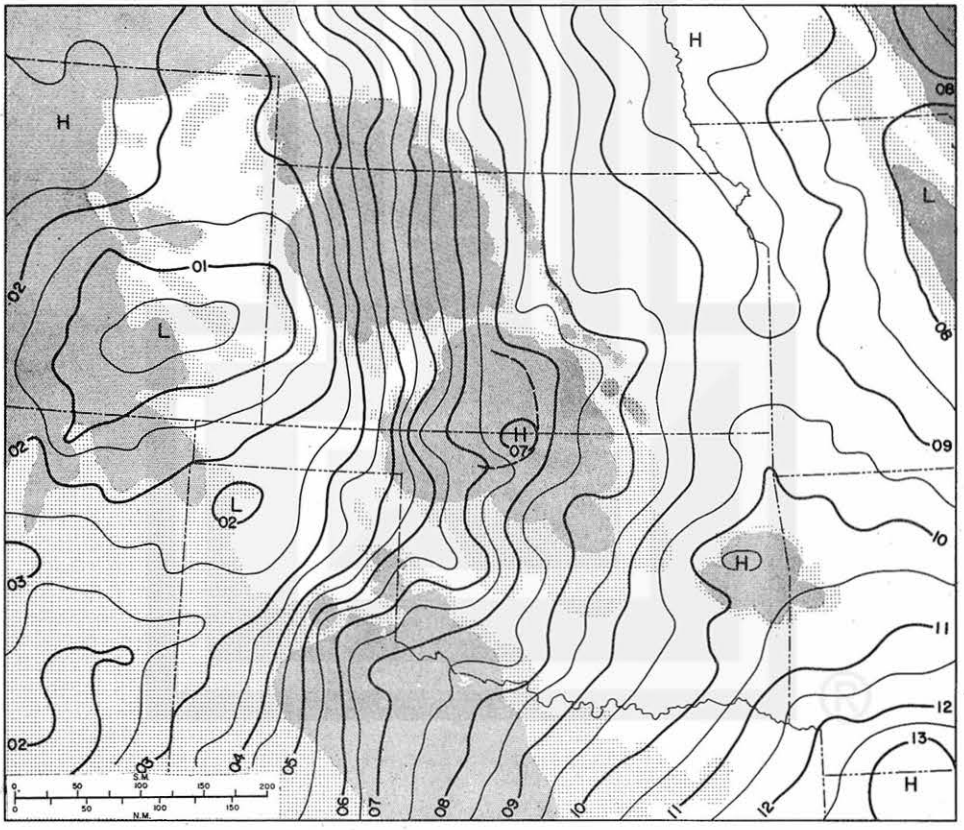

Fig. 15 Machine analysis at 1719 CST, May 27, 1960, with clouds photographed by Tiros I at this time. Dashed line shows location of pressure jump line.

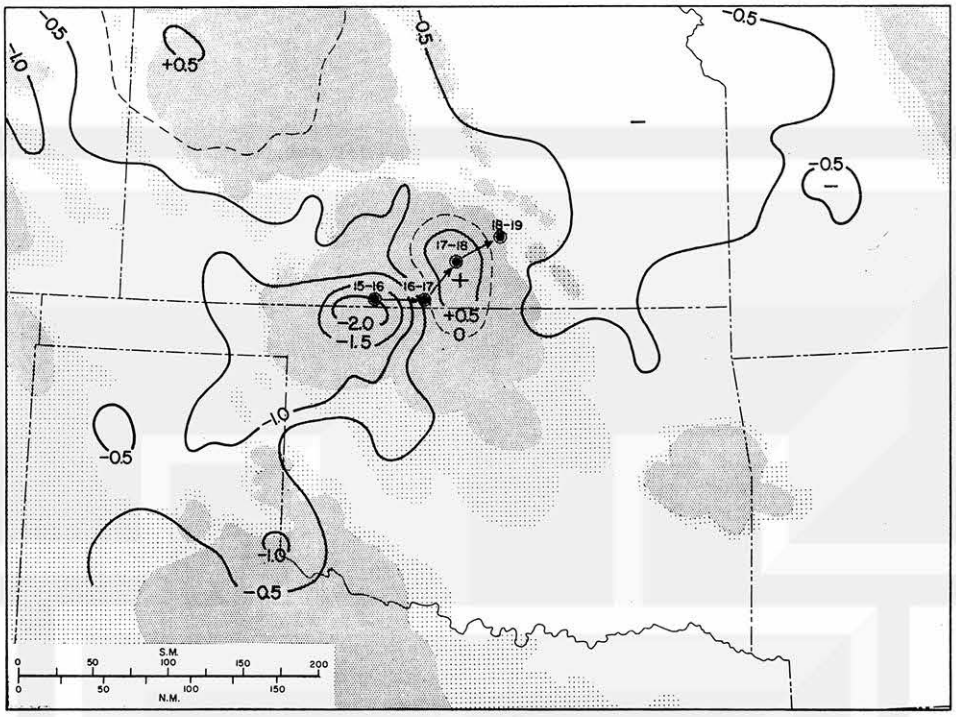

Fig. 16 Pressure change chart, 1700 CST to 1800 CST, May 27, 1960, from machine analyses, and track of centers of hourly, positive pressure change in mb.

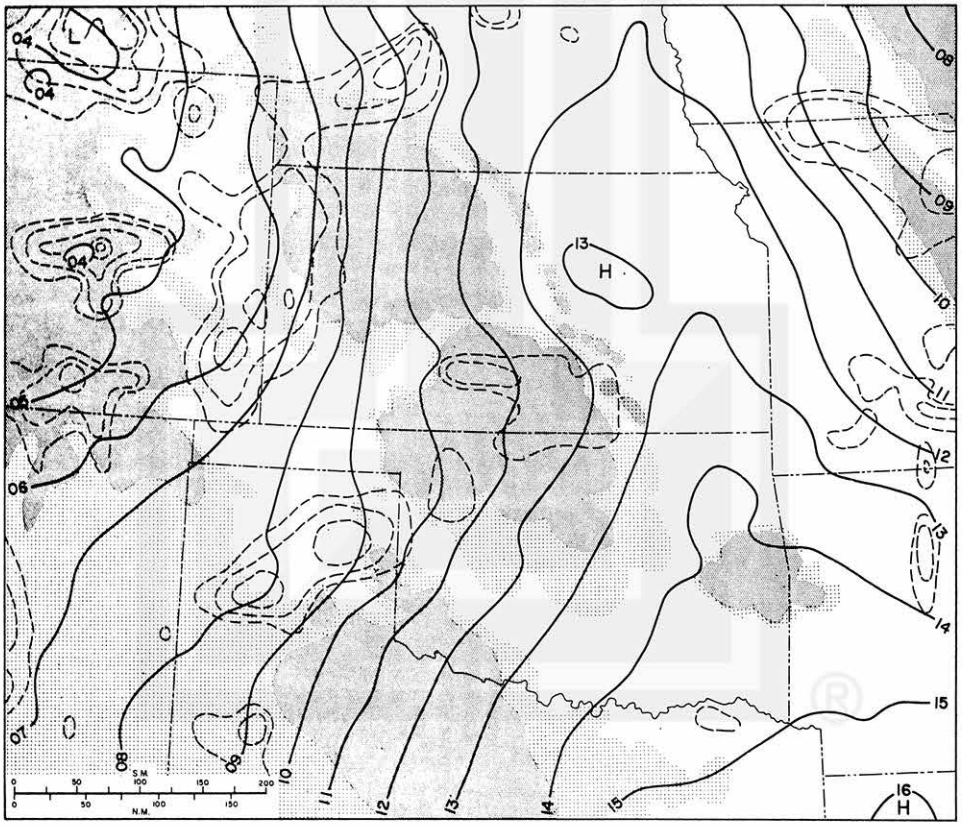

Fig. 17 Machine pressure analysis at 1200 CST, May 27, 1960, the Laplacian of the pressure field or equivalent relative geostrophic vorticity (outline of positive values only) and Tiros clouds at 1719 CST.

is due both to the size of the systems involved in this case and the fact that, in its present form, the program analyzes for point values of pressure at the stations with linear interpolations between stations, as explained, and does not reproduce the true gradients between stations. Nevertheless, the resulting analyses qualitatively show the major mesoscale features as well as their development and movement.

The preceding analyses focus attention on the pressure patterns associated with the cloud mass detected along the Oklahoma-Kansas border by the Tiros satellite. The development of mesohighs associated with the other cloud systems, only slightly underway at 1719 CST, continued through midnight, at which time there is evidence of four dintinct high pressure systems ranging from western Nebraska into northern Texas.

B. Relative Geostrophic Vorticity and Cloud Patterns

In an effort to further relate these seemingly minor systems to the cloud patterns photographed, a method of computing an equivalent relative geostrophic vorticity was devised, similar to that used recently by Siler (1962). Basically it consisted of evaluating the Laplacian of the pressure field by finite differences, i.e., of summing the grid values to the north, east, south and west of a point and subtracting four times the value at the point. This is a method commonly used in meteorological computation schemes. To obtain the relative geostrophic vorticity it is necessary to multiply by $g/(fd^2)$, where g is the acceleration of gravity, f, the Coriolis parameter and d, the spacing between grid points. Because of the narrow range of latitudes involved, this refinement was not necessary for the results obtainable at this time.

Results of this operation showed a rather irregular field of data for which some areas were dominated mostly by negative values and some mostly by positive values, but with considerable amount of opposite signs interspersed. These appear due to the unsystematic selection of triangles of stations in the objective analysis scheme, which is currently being modified to improve the analysis. A method to smooth out these unrepresentative values was adopted: simply to sum the values at each grid point with the values at the eight nearest ones forming a square surrounding it, to produce a new value

of the equivalent relative geostrophic vorticity at the point. Division by nine to form average values is not necessary, since patterns rather than absolute values are required here.

In printing a grid of this vorticity field, negative and small positive values were eliminated to show more clearly the relationship of the significant positive areas to the areas occupied by the cloud masses photographed.

The results appear quite significant. In Fig. 17, based on the analysis for 1200 CST, maximum values are arranged essentially in two parallel SW-NE oriented bands at noon, shortly before the onset of thunderstorm activity. One extends from eastern Colorado though extreme western Kansas into Nebraska. The other extends through the Texas Panhandle into south-central Kansas. Two definite maxima appear in eastern Colorado and the Texas Panhandle, in positions quite well correlated with the two distinct cloud masses photographed by the satellite five hours and nineteen minutes later.

The vorticity patterns underwent changes in shape and extension over the next five hours but maxima at 1200 CST virtually remained in the same locations (generally within 50-75 miles) throughout this period. In this next figure, for 1719 CST (Fig. 18), the time of the Tiros photograph, the area of positive equivalent geostrophic vorticity still shows a distinct cellular relationship corresponding to the two main cloud masses, with the centers of the cloud masses displaced downwind (northeastward) by about 125 miles.

It appears likely that the winds at or near the gradient level, moving through the slow-moving area of maximum relative geostrophic vorticity would be subject to convergence resulting in upward vertical motion near the ground which may give rise to the cloud masses themselves. Similarly, mesohighs which appear beneath the cloud masses must be expected to possess negative values of relative geostrophic vorticity. However, the general lack of clouds in the areas of positive relative vorticity indicates the entire explanation cannot be found on the basis of surface pressure data alone. In general, the locations of the positive relative vorticity areas correlate extremely well with the absence of clouds in the photograph.

Figure 19 shows the development of the individual mesosystems by 0000 CST, May 28, 1960, and the development of the equivalent relative geostrophic vorticity pattern in

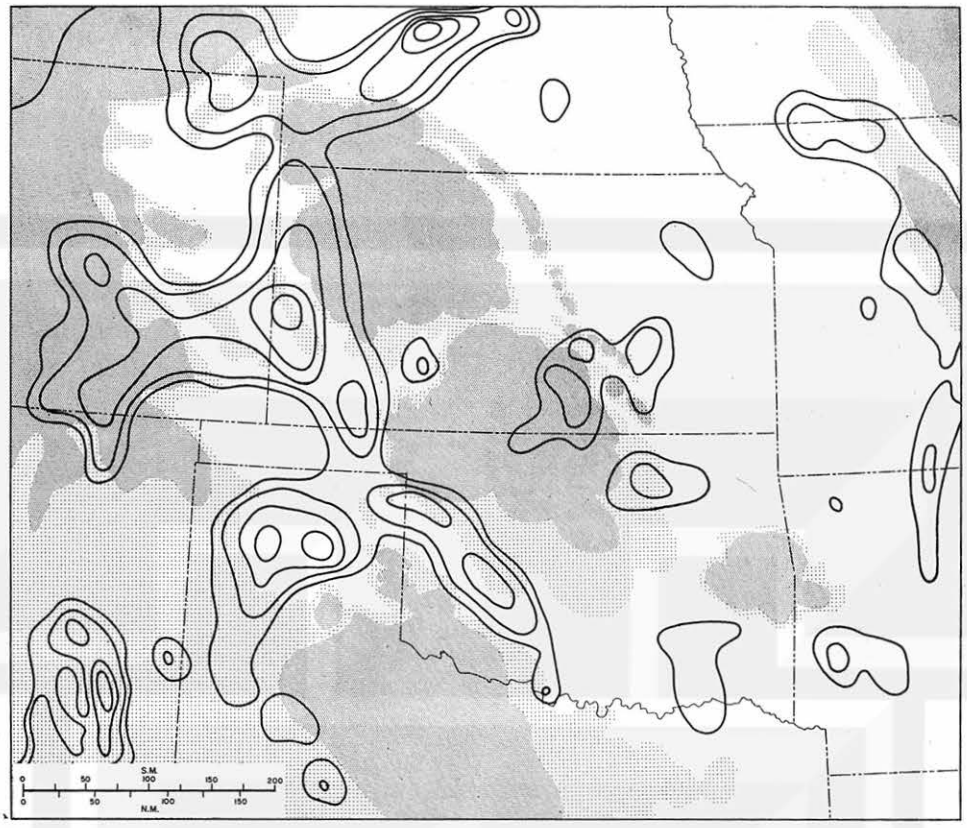

Fig. 18 Laplacian of the pressure field (outline of positive values only) at 1719 CST, May 27, 1960, with clouds photographed by Tiros I at this time.

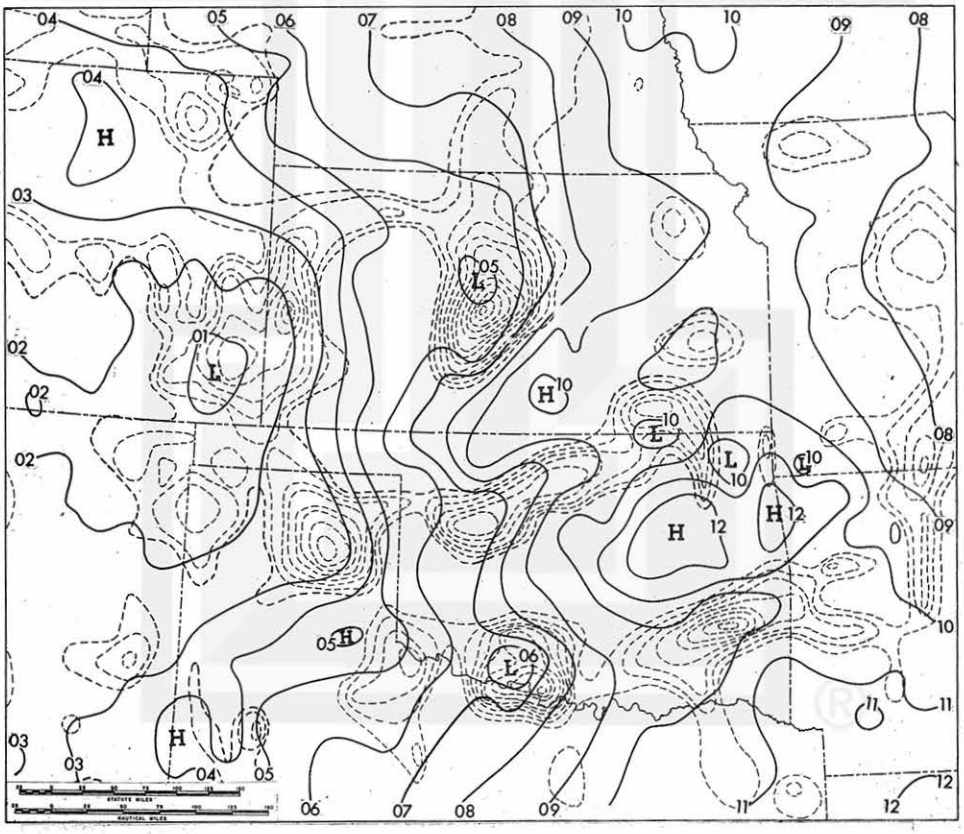

Fig. 19 Pressure analysis and Laplacian of the pressure field (outline of positive values only) at 0000 CST, May 28, 1960.

relationship to them. The pressure pattern has become quite irregular at this time. The geostrophic vorticity field bears little resemblance to the patterns at 1200 CST and 1719 CST with positive values concentrated along troughs which evidently mark the divisions between individual mesohighs or their associated ridges. Several centers have become much more intense than the initial centers at 1200 CST. Four distinct mesosystems are defined by the isobars and vorticity patterns. One in southwestern Nebraska, a small one in western Kansas, an elongated one along the Kansas-Oklahoma border bending northeastward toward eastern Kansas, and a fourth extending entirely across central Oklahoma from the Texas Panhandle and bending northeastward into northwestern Arkansas.

It appears that the sea level areas of maximum relative geostrophic vorticity are instrumental in initiating the release downstream of convective instability quite early in the life of the mesosystem. As the mesohighs appear, associated negative values of the relative geostrophic vorticity develop underneath the cell and the areas of positive values tend to extend and intensify between the cells. By this time the winds are usually sufficiently agestrophic so that there is little relationship between actual and geostrophic relative vorticity. The genetical properties of the positive areas therefore become meaningless, but by continuing to analyze them we are able to define the boundaries of the mesohighs by numerical means. As applied to the present initial study, this technique produces results that agree very well with convective cloud systems photographed by a satellite.

IV. INFRA-RED RADIATION FROM MESOSCALE NEPHSYSTEMS

A. Concept of Plotting Radiation Data on Cloud Photographs

Extensive research was done in developing a method of plotting radiation data directly on each cloud photograph, whereby the data can be contoured on the photo-

graph. Researchers, thus, can easily identify the objects which are the sources of radiation under investigation.

It is not the scope of this paper to explain in full the method of plotting radiation data on cloud photographs. The method is, however, an extension of a technique for precise rectification of satellite cloud photographs developed by Fujita (1961). Only one grid, the "radiometer grid," is required in addition to the ones required for the rectification of cloud photographs. They are the Nadir Angle, Height, Fiducial, and Distortion-free fiducial grids; the OEC projection chart for proper angle of orbital inclination and its overlay.

The terrestrial radiometer-axis point, TRA, is defined as the point at which the axis of radiometer aperture penetrates the surface of the earth. As a result of the spinning and translational motions of the satellite, TRA moves over the earth's surface forming "swath lines." The aperture of the scanning radiometer is 5 degrees for Tiros II and III, thus, the sensor integrates the radiation from the area surrounding the TRA. As a result, the area of radiation measurement extends on both sides of the swath line. This narrow band of radiation measurement on the earth is called "swath."

First, we plot a series of TSP's at the time when TRA crosses the principal line. During one spin of the satellite, TRA crosses both the earth and the outer-space sides of the principal line as viewed from the TPP. We take the earth side crossing time to minimize the error resulting from the following assumption. It is assumed that the TSP remains at the same point while TRA moves from its position at the maximum object nadir angle to the minimum and then to the maximum. At the end of one complete spin, TSP translates instantly to the next spin position, and so forth.

The movement of the radiometer-axis point on image, IRA, can be obtained by superimposing the radiometer grid on the proper nadir angle grid in such a manner that the principal points and the principal lines on these two grids coincide. Now, the circle formed by IRA on the nadir angle grid is transcribed onto an OEC chart with the help of a proper height grid. The track of TRA, thus obtained, is the swath line which takes approximately the shape of either a circle, an ellipse, a parabola or a hyperbola depending upon the nadir angle at the moment of the spin. We may plot the radiation data along the swath lines on an OEC chart, however, they can be transcribed onto any

synoptic map or even onto cloud photographs before data plotting is undertaken.

Presented in Fig. 20 is a cloud photograph over the Northwestern tip of South America. The coast lines and geographic grids were added later. Several significant spots in the photograph are designated as C(cirrus), F(foehn region), H(hurricane), M(mountains), and N(mesoscale nephsystems) and numbered 1, 2, 3,... for identification purposes.

The topographic features shown by the 1000-and 3000-meter contour lines drawn on the photograph are reproduced in Fig. 21. A rather interesting fact seen in the figure is the geographic location of dark areas designated as F1, F2, F3, F4, and F5, which are visible to the east of mountains such as Sierra de Perija, Cordillela de Merida, Cordillela Orienta, and Cordillela Central. We suspect that these areas were dominated by westerly winds while the Caribbean Sea was under the influence of easterlies. The intertropical front was, therefore, extended in the vicinity of 10^{o}N latitude where a number of large convective nephsystems and Hurricane Anna were located.

Depicted in Fig. 22 is the amount of reflection from clouds and terrain tops. The numbers attached to the intensity contours are uncalibrated scales appearing on the radiation analog trace of Channel 5. The trace registered scale 10 consistantly when the sensor pointed to outer space; on the other hand, the brightest cloud in the photograph indicated approximately 40 scales. Between these two extreme scales, fifteen-intensity contours were obtained.

There was considerable limb-darkening near the apparent horizon. In other areas, however, the reflection intensity patterns showed a remarkable agreement with the brightness of clouds and terrain in the photograph. It is of interest to find that a white mass of nephsystem at the upper right corner of the photograph was characterized by an extremely large reflectivity. Channel 2 data from this system revealed that its temperature was very low. Nephsystems N1, N2, and N3 were also very bright in comparison with the white areas over mountainous terrain.

Radiation patterns of Channel 2 data registered 14 scales while pointing to outer space and 85 scales from the cloudless Caribbean-Sea surface. Fifteen levels of

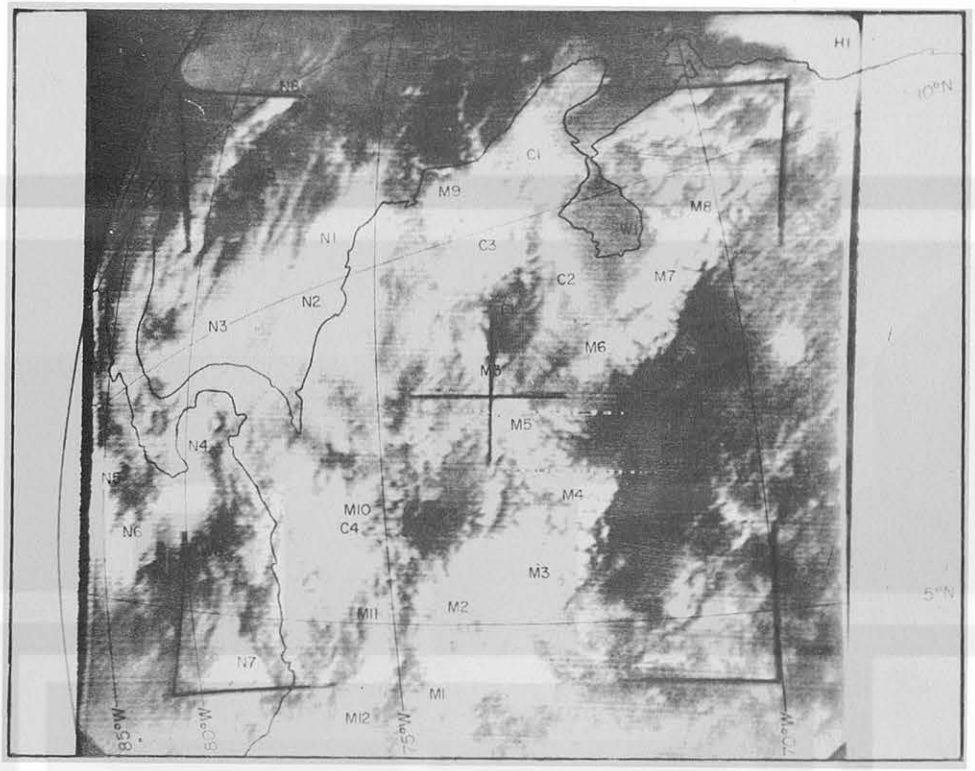

Fig. 20 Frame 2T, Orbit 118, Tiros III. Technical information: Exposure time - 16h 25m 48s GMT, July 20, 1961; Satellite subpoint - 6.2°N, 70.0°W; Altitude - 784 km; Nadir angle - 27.5°; Azimuth angle - 289°.

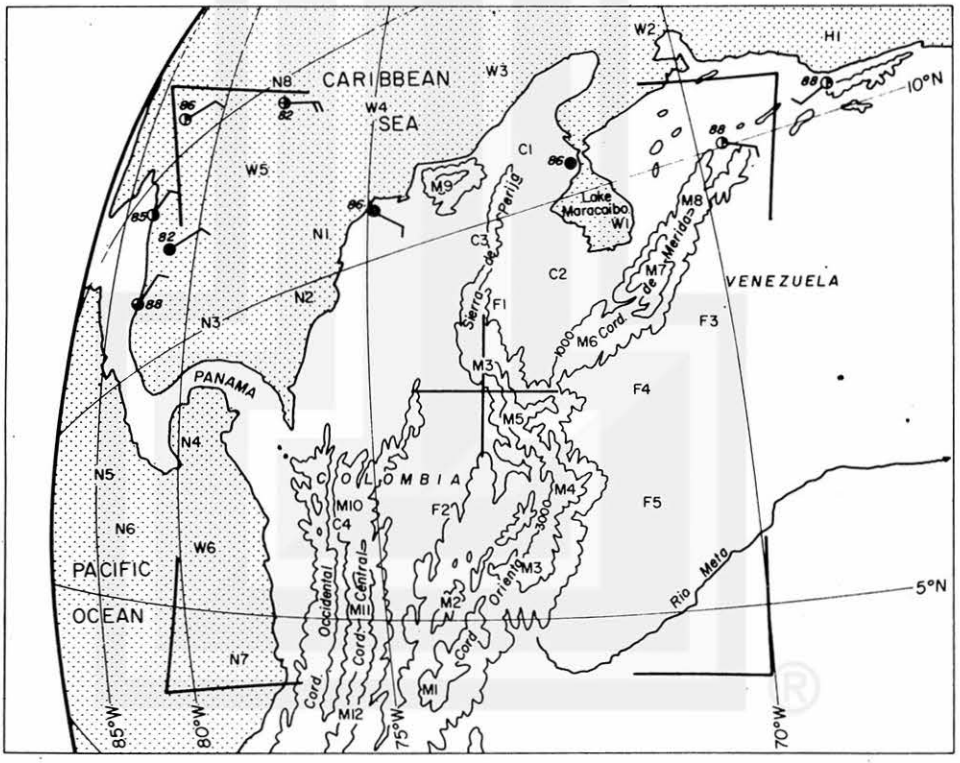

Fig. 21 Geographical features which are to be superimposed on the Tiros III photograph, Frame 2T, orbit 118. Topography is shown by 1000-and 3000-meter contour lines. Surface weather at 1800 GMT, July 20 also appears in the figure.

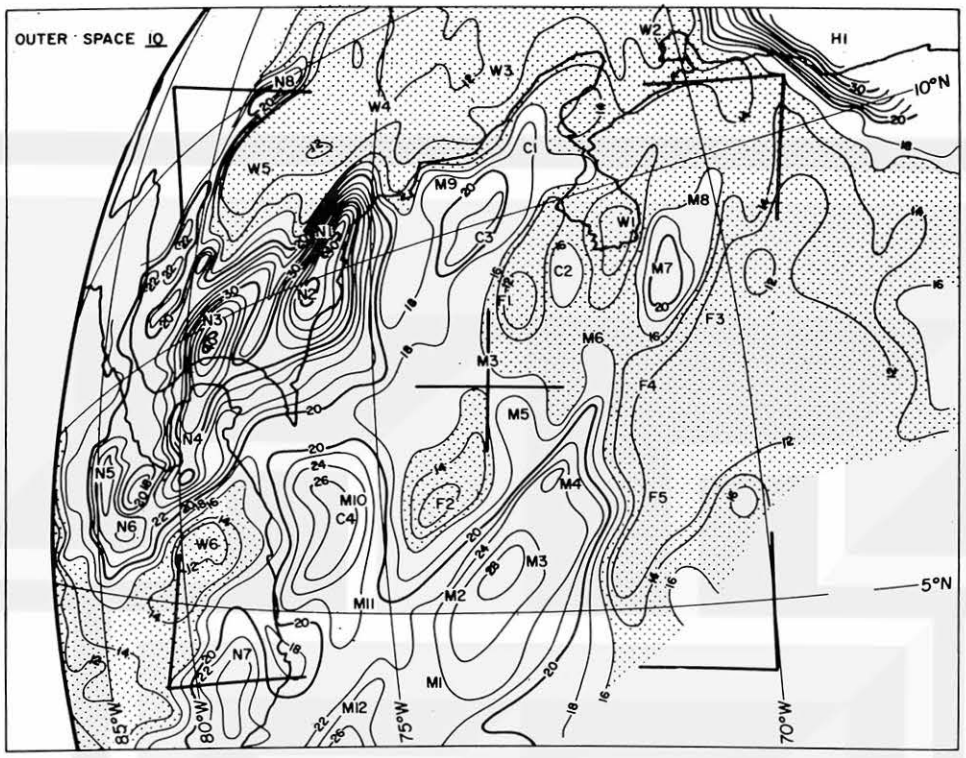

Fig. 22 Intensity of reflection as determined by Channel 5 radiation data. Numbers on the intensity contours are the same as the scales on the analog trace which indicate 10 scales while pointing to outer space. No calibration was made.

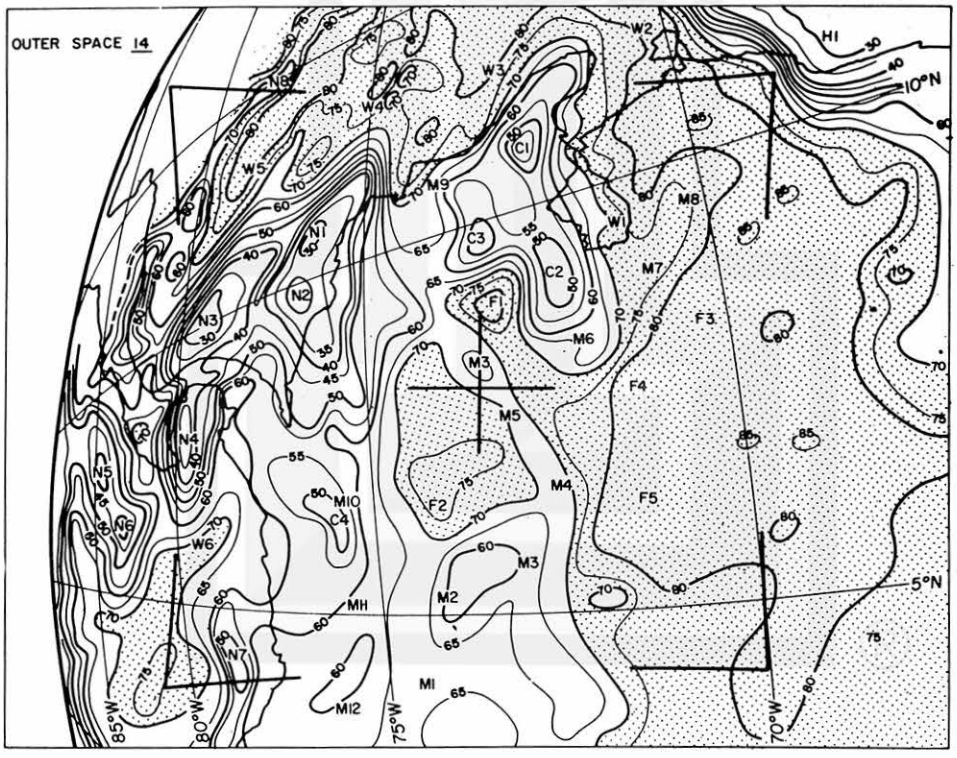

Fig. 23 Uncalibrated intensity contours ofChannel 2 data. Large nephsystems such as N_1, N_2, ... appeared to be very cold. Even small patches of faint cirrus, C_1, C_2, indicate much lower radiation values than those from the high Andes Mountains.

radiation intensity shown in Fig. 23 were depicted on the cloud photograph. As expected, the areas of foehn are relatively warm and the mountain tops covered by orographic cumuli are colder than surrounding planes. Two areas of faint clouds, seen to the northwest and southwest of Lake Maracaibo, indicated a much colder temperature than the extreme white area over Merida Mountains to the southeast of the lake. It is therefore, reasonable to presume that the two faint reflection areas were caused by high clouds such as cirrus or cirrostratus. Thus, the atmospheric window channel reveals that the hurricane cloud indicates at H1 was very cold despite the fact that it is not very outstanding in the photograph, and that the nephsystems N1 through N4 near Panama were the large masses of cirrus diverging out from cumulonimbi extending into high levels. The effect of limb-darkening is apparent for nephsystems N5 and N6 which existed near the apparent horizon.

B. Radiation-Reflection Diagram

Radiation and reflection intensities plotted directly on cloud photographs reveal important characteristics of the radiation from each object, such as clouds, mountains, etc. Figure 24 showing Channel 2 data and topography combined, tells us of the existence of small patches of cold or low radiation areas directly over mountains covered partially or entirely with orographic clouds. These patches, irregular in shape and rather permanent in position, should preferably be eliminated, as long as we are interested in traveling mesoscale nephsystems. The philosophy behind this is similar to that of "ground clutter" in the study of traveling radar echoes. It is proposed that such orographic noise in radiation be called "mountain clutter", examples of which appear in Fig. 24 over Sierra Guanay (southeast corner), Cordillera de Merida and Cordillera Orienta (center to southwest). Even if it is not feasible, as in the case of radar ground clutter, to eliminate mountain clutter entirely, it is better to investigate convective nephsystems after reducing the amount of mountain clutter. Original figures of radiation data used in drawing the Channel 2-contour lines appear in Fig. 25.

An attempt was made to summarize the Channels 2 and 5 data from different objects appearing in the photograph under discussion. The result is tabulated in Table II, and

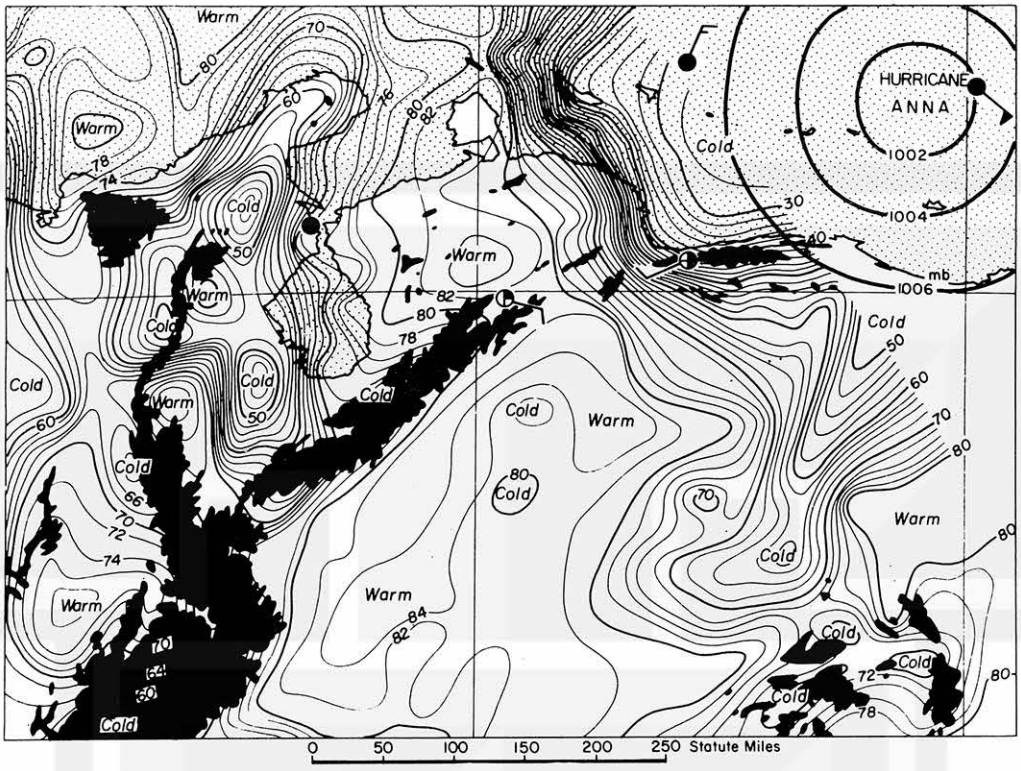

Fig. 24 Precise rectification of Channel 2 data over the northern tip of South America. The radiation scales labeled on the intensity contours are the same as those used in Fig. 23.

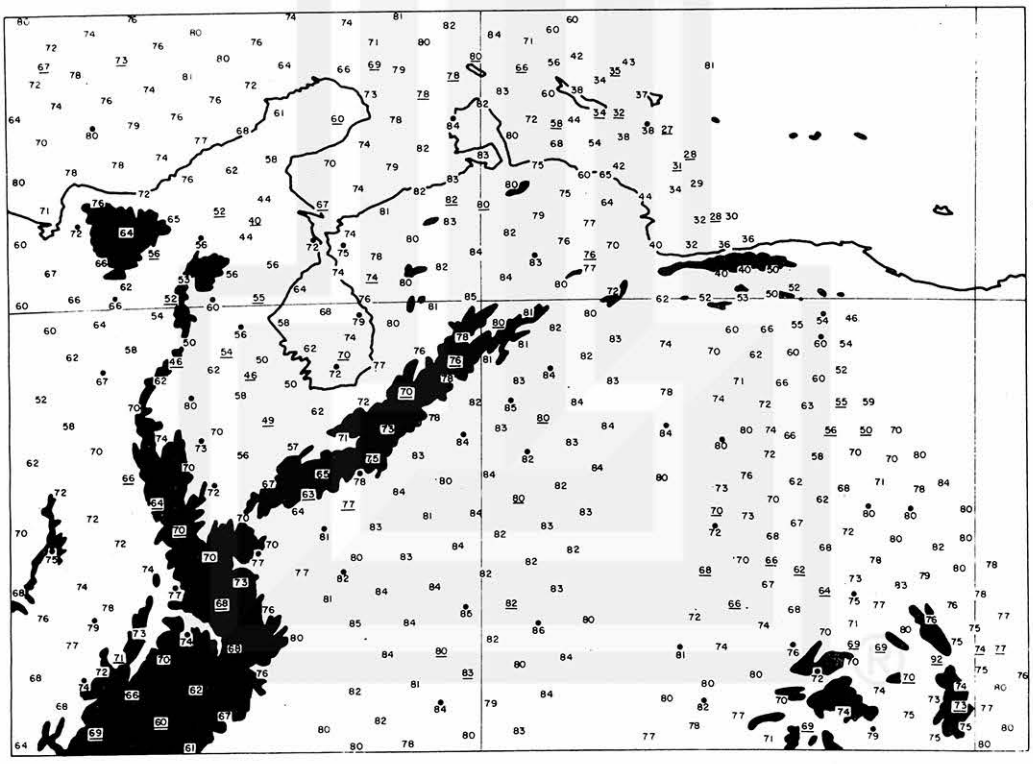

Fig. 25 Uncalibrated radiation values plotted at the data points along swath lines. Underlined numbers represent minimum values and those with a dot on top indicate maximum values along each swath line.

plotted on the radiation (Channel 2) and reflection (Channel 5) diagram shown in Fig. 26. It was found that groups of similar objects are distributed over localized areas of the Channel 2-5 diagram. Careful examination of this diagram suggests that a type of convection involving ice crystals completes a large cycle involving "ice-crystal nephsystems." Such nephsystems may form over oceans, plains, or mountains and may quickly grow both in height and horizontal dimensions until reaching the upper left tip of the cold convection cycle. During the dissipating stage, the high clouds from the cold tops diverge out and diffuse into cirriform layers. As the average size of ice crystals decreases and they become further apart, reflection is reduced and Channel 2 radiation from underlying layers passes through the high cloud layers, resulting in the increase of effective blackbody temperature of the dissipating clouds. Three patches of faint cirrus C1, C2, and C3 in the photograph would represent such a stage.

When convective clouds remain water stages, the radiation and reflection is characterized by those from water clouds, and this type of cloud may be called "water nephsystem" in contrast with the ice-crystal nephsystem. When measuring radiation from water nephsystems, Channel 2 data does not drop as in the case of ice-crystal nephsystems, while the increase in reflectivity takes place mainly as a result of larger cloud coverage as individual nephelements analgamate. A typical cycle involving water clouds shown in Fig. 26 indicates that the effective blackbody temperature estimated by Channel 2 data is much warmer than that of ice-crystal nephsystems with similar reflectivity in Channel 5 spectrum.

Despite the fact that this statistical study was done by using only one frame of Tiros III photographs the result turned out to be rather encouraging. It is evident that this type of study using different photographs over various geographic locations and meteorological conditions is useful in learning the radiation characteristic of mesoscale convective nephsystems.

OBJECT	Symbol	Channel 2	Channel 5	Feature on Cloud Photograph
Outer Space		14	10	Black
Cirrus	C1	40	18	Faint white 30x50 miles in area
	C2	46	16	Faint white 30x40 miles in area
	C3	46	21	Faint white, orographic Cu superimposed
Mountain	M1	66	24	4500m 7/10 cloud cover
	M2	60	26	3500m 8/10 cloud cover
	M3	61	26	3200m 9/10 cloud cover
	M4	68	23	5400m 6/10 cloud cover
	M5	70	18	3500m 6/10 cloud cover
	M6	65	14	3100m 3/10 cloud cover
	M7	75	22	5000m 9/10 cloud cover
	M8	78	17	3100m 8/10 cloud cover
	M9	64	18	5700m 6/10 cloud cover
	M10	51	25	3000m 7/10 cloud cover
	M11	64	22	5200m 2/10 cloud cover
	M12	61	24	5500m 6/10 cloud cover
Water	W1	74	12	Black on cloud photograph
	W2	83	12	Black on cloud photograph
	W3	80	11	Black on cloud photograph
	W4	78	12	Black on cloud photograph
	W5	82	10	Black on cloud photograph
	W6	74	10	Black on cloud photograph
Nephsystem	N1	29	41	60x 60 miles in area
	N2	28	40	100x100 miles in area
	N3	24	36	30x100 miles in area
	N4	34	30	40x 50 miles in area
	N5	34	26	50x 50 miles in area
	N6	40	26	30x 50 miles in area
	N7	46	24	50x100 miles in area
Foehn	F1	80	10	40x 60 miles in area
	F2	77	12	50x 70 miles in area
	F3	84	10	60x 80 miles in area
	F4	83	10	80x120 miles in area
	F5	82	10	80x120 miles in area
Hurricane	H1	28	34	Hurricane Anna

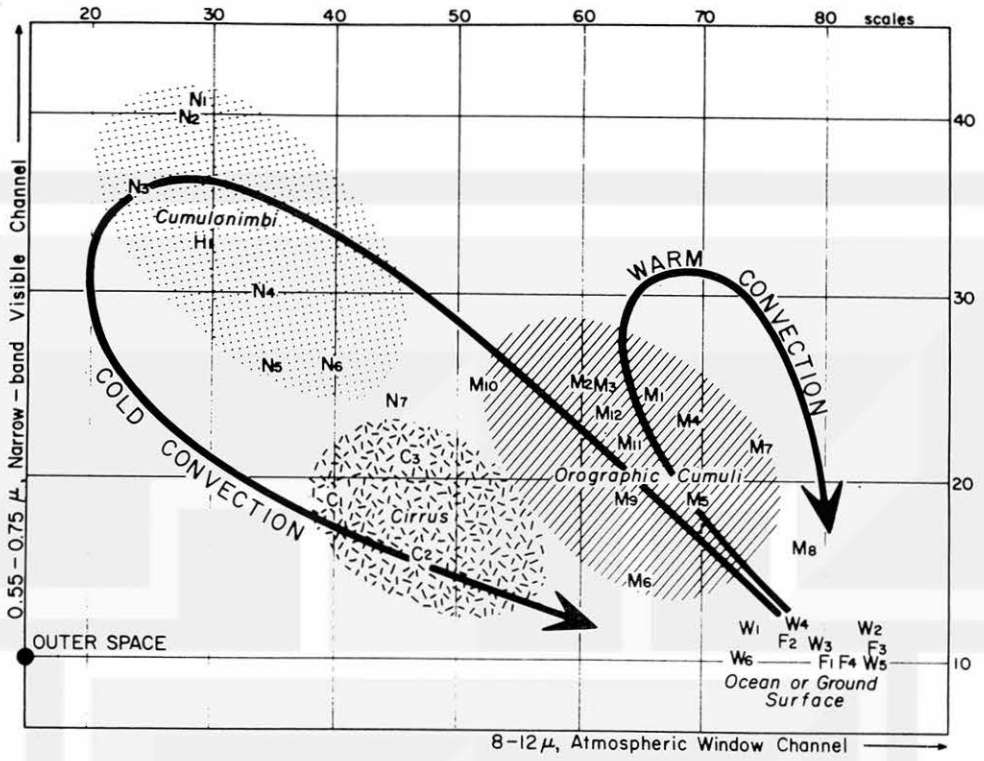

Fig. 26 Two types of convection seen on a radiation-reflection diagram. Convections involving ice-crystal clouds and water clouds are designated as cold and warm convections.

V. CONCLUSIONS

As a result of this research, it was learned that the photographic and radiation data from the Tiros series of meteorological satellites are very useful in the physical and dynamical interpretation of convective nephsystems ranging from isolated cumulonimbus to organized hurricane clouds.

The first part of the research relating Tiros clouds and radar echoes brought up the problem of identifying cumulonimbus cells using Tiros photographs. It has been known that the resolution of the present satellite is high enough to identify convection cells imbedded inside the nephsystems which are free from large decks of overhanging high clouds. When the associated anvil clouds spread out considerably, the whole nephsystem observed from Tiros turns into a white mass which may include

a number of convective cells equivalent to those photographed with ground located radar. Even a small plume on a satellite photograph was found to include several cells of radar echoes. In view of this, it is hardly possible to obtain the areas of convective towers hidden beneath the cirrus deck of giant nephsystems.

The second part of the research involved the interpretation of Tiros nephsystems and machine-produced mesoanalysis charts over a specially instrumented network. It was learned that the sea-level pressure patterns, including mesohighs and mesolows, analysed by the machine are not significant enough to relate quantitatively with cloud patterns characterized by large masses of nephsystems. However, the Laplacian of the sea-level pressure computed by finite difference from a 22.0 N. M. grid revealed the existence of large positive values. That is to say, the areas of positive relative vorticity are characterized by the lack of clouds. This indicates an opposite result from the cases of regular synoptic systems in which more clouds are usually seen over the area of positive relative vorticity. We should realize, however, that cloud distribution in relation to pressure systems changes appreciably when the scale becomes small. The results, thus obtained, seem to be reasonable, since we used to observe more clouds over mesohighs than over the areas between them. It is of interest to find the machine-produced Laplacian to be useful in determining the cloudless areas associated with the mesoscale convection.

Finally, the radiation data from Tiros III were investigated by plotting them on cloud photographs. An extremely careful analysis is required in determining data points on Tiros photographs. Once plotting is done, however, the radiation data are contoured directly on each photograph permitting us to identify the sources of reflection and emission precisely. Despite the fact that this radiation data analysis is still in a research stage, we feel that future mechanization will cut down the plotting time considerably to the extent that radiation charts for various channels will be prepared even for operational use.

ACKNOWLEDGEMENTS

The authors are grateful to the staff members of the Mesometeorology Project, Department of the Geophysical Sciences, University of Chicago for their assistance in this research. The microbarograms were evaluated by Mr. George W. Hollenbaugh, United States Weather Bureau, whose skill and careful attention to details of the traces contributed much to the quality of the machine analysis.

Sincere appreciation should be expressed to Dr. Morris Tepper and Mr. Charles P. Wood of the National Aeronautics and Space Administration; Mr. Linwood Whitney, Jr. of the Meteorological Satellite Laboratory, United States Weather Bureau; and to Mr. Roy H. Blackmer of Stanford Research Institute, for their useful suggestions and assistance in the completion of this research.

REFERENCES

Blackmer, R. H. Jr., 1961: Satellite observations of squall line thunderstorms. Proc. 9th Wea. Radar Conf., 76-82.

Dellert, G. T. Jr., 1962: Data processing procedures in numerical mesoanalysis. Mon. Wea. Rev., 90, 133-146.

Fritz, S., and H. Wexler, 1960: Cloud pictures from satellite Tiros I. Mon. Wea. Rev., 88, 79-87.

--------, and J. S. Winston, 1962: Synoptic use of radiation measurements from Tiros II. Mon. Wea. Rev., 90, 1-9.

Fujita T., 1961: Outline of a technique for precise rectification of satellite cloud photographs. Res. Paper 3, Mesomet. Proj., Univ. of Chicago.

--------, and T. Ushijima, 1961: Investigation of squall lines with the use of radar and satellite photographs. Proc. 9th Wea. Radar Conf., 186-192.

Hitschfeld, W., 1960: The motion and erosion of convective storms in severe vertical shear. J. Meteor., 17, 270-282.

Nordberg, W., W. R. Bandeen, B. J. Conrath, V. Kunde, and I. Persano, 1962: Preliminary results of radiation measurements from the Tiros III meteorological satellite. J. Atmos. Sci., 19, 20-30.

Siler, R. K., 1962: Synoptic patterns for wet and dry trades in the Island of Hawaii. Mon. Wea. Rev., 90, 103-106.

Stroud, W. G., 1961: Meteorological measurements from the Tiros satellites, Lecture Paper, International Meteorological Satellite Workshop, Washington, D.C.

Whitney, L. F. Jr., and S. Fritz, 1961: A tornado-producing cloud pattern seen from Tiros I. Bull. Amer. Meteor. Soc., 42, 603-614.

MESOMETEOROLOGY PROJECT ----- RESEARCH PAPERS

1. Report on the Chicago Tornado of March 4, 1961 - Rodger A. Brown and Tetsuya Fujita

2. Index to the NSSP Surface Network - Tetsuya Fujita

3. Outline of a Technique for Precise Rectification of Satellite Cloud Photographs - Tetsuya Fujita

4. Horizontal Structure of Mountain Winds - Henry A. Brown

5. An Investigation of Developmental Processes of the Wake Depression Through Excess Pressure Analysis of Nocturnal Showers - Joseph L. Goldman

6. Precipitation in the 1960 Flagstaff Mesometeorological Network - Kenneth A. Styber

7. On a Method of Single-and-Dual-Image Photogrammetry of Panoramic Aerial Photographs - Tetsuya Fujita

8. A Review of Researches on Analytical Mesometeorology - Tetsuya Fujita